Chinese Chemical Letters 35 (2024) 108641

Contents lists available at ScienceDirect

Chinese Chemical Letters

journal homepage: www.elsevier.com/locate/cclet

Bismuth-based halide double perovskite Cs_2KBiCl_6: Disorder and luminescence

Pan Liu[a], Yanming Sun[a], Alberto J. Fernández-Carrión[a], Bowen Zhang[a], Hui Fu[b], Lunhua He[c,d,e], Xing Ming[f], Congling Yin[a,*], Xiaojun Kuang[a,g,*]

[a] MOE Key Laboratory of New Processing Technology for Nonferrous Metal and Materials, Guangxi Key Laboratory of Optic and Electronic Materials and Devices, College of Materials Science and Engineering, Guilin University of Technology, Guilin 541004, China
[b] Analytical Instrumentation Center, College of Chemistry and Molecular Engineering, Peking University, Beijing 100871, China
[c] Spallation Neutron Source Science Center, Dongguan 523803, China
[d] Chinese Academic of Science, Institute of Physics, Beijing National Laboratory for Condensed Matter Physics, Beijing 100190, China
[e] Songshan Lake Materials Laboratory, Dongguan 523808, China
[f] College of Science, Guilin University of Technology, Guilin 541004, China
[g] College of Chemistry and Bioengineering, Guilin University of Technology, Guilin 541004, China

ARTICLE INFO

Article history:
Received 18 April 2023
Revised 4 May 2023
Accepted 31 May 2023
Available online 2 June 2023

Keywords:
Halide perovskite
Double perovskite
Luminescence
Disordered structure
Direct bandgap

ABSTRACT

A new bismuth-based halide double perovskite Cs_2KBiCl_6 was isolated successfully through solid-state reactions and investigated using X-ray and neutron diffraction. Rather than an ordered structure, the crystal structure consists of shifted Cs, K, Bi, and Cl sites from the ideal positions with fractional occupancy in compensation, leading to variable local coordination of Cs^+ ions, as revealed by ^{133}Cs solid-state nuclear magnetic resonance spectroscopy. Cs_2KBiCl_6 displays volume hysteresis at 5–298 K range upon heating and cooling. The Cs_2KBiCl_6 has a direct bandgap of 3.35(2) eV and red-shift luminescence of around 600 nm upon Mn doping compared with the Na analogue. The stabilization of disordered structure in Cs_2KBiCl_6 is related to two factors including the large-sized K^+ cation which prefers to coordinate with more than six Cl^-, and the Bi^{3+} with $6s^2$ lone pair which has a preference for a local asymmetric environment. These findings could have general application and help to understand the structure and property of halide perovskites.

Hybrid lead halide perovskites $APbX_3$ ($A = CH_3NH_3^+$, $HC(NH_2)_2^+$; $X = Cl^-$, Br^-, I^-, Fig. S1a in Supporting information) had been the keystones of the next-generation solar cells as light absorbers and attracted worldwide attention in last decades [1–3]. However, concerns about the toxicity and stability of the lead-containing materials have stimulated a great deal of interest in the discovery of nontoxic and stable perovskites that might be equally effective as the parent lead halides [4–7]. One of the strategies for achieving this has been to synthesize cesium-based double perovskite (DP), of general formula $Cs_2M^IM^{III}X_6$ (where M^I and M^{III} are univalent and trivalent metals at the Pb site, and X is a halide anion, Fig. S1b in Supporting information), including examples such as $Cs_2AgBiCl_6$ [4,6,8,9], $Cs_2AgSbBr_6$ [10] and $Cs_2NaBiCl_6$ [11–13]. Among these Cs-based DPs, the Bi-containing materials display band structures broadly similar to those of the lead halide perovskites, since the substituted Bi(III) has $6s^2$ electronic configuration similar to Pb(II). Therefore, Bi-based DPs are seen as promising alternatives for lead halide perovskite.

Apart from solar absorbers, these halide DPs have favorable optoelectronic performances for applications such as photodetectors [8,14], scintillators [15,16], and phosphors [17–21]. Thus, the interest in the halide DPs, especially the Bi−based materials, has been continuously growing [4,6,8,12,22–25]. Although far more Bi-based halide DPs were predicted by theoretical studies, only three chloride $Cs_2M^IBiCl_6$ (M^I = Li, Na, and Ag) and one bromide $Cs_2AgBiBr_6$ have been isolated experimentally as stable crystalline phases so far. The Bi-based iodide DPs are unstable under normal conditions [26]. For instance, the Cs_2AgBiI_6 DP can only be prepared as kinetically stabilized nanocrystals by post-synthetic modification of the corresponding chloride and bromide [27]. The reports of Cs_2NaBiI_6

* Corresponding authors at: MOE Key Laboratory of New Processing Technology for Nonferrous Metal and Materials, Guangxi Key Laboratory of Optic and Electronic Materials and Devices, College of Materials Science and Engineering, Guilin University of Technology, Guilin 541004, China.
E-mail addresses: congling.yin@glut.edu.cn (C. Yin), kuangxj@glut.edu.cn (X. Kuang).

https://doi.org/10.1016/j.cclet.2023.108641
1001-8417/

DP have not been substantiated by definitive structural characterization [28].

In addition, the Bi-based chloride DPs suffer from instability issues. For example, the $Cs_2CuBiCl_6$ compositions cannot form perovskite structures in contrast with its Ag analogs. Such difference in stability comes from the fourfold coordination preference of Cu^+ ion with halide ions, dissatisfying the sixfold coordination requirement in the DPs [29]. Another example is extremely moisture-sensitive $Cs_2LiBiCl_6$ DP. This instability is related to small-sized Li^+ cation, which degrades from sixfold to lower coordination irreversibly upon the moisture attack [25].

Although the rare-earth-based DPs $Cs_2KM^{III}Cl_6$ (M^{III} = Sc, Eu, Lu) were first reported in the 1990s [30,31], little attention was paid to the Bi-based halide DPs containing a large alkali metal cation K^+ (Cs_2KBiCl_6) except a pioneer experimental study on the nanocrystals of Cs_2KBiCl_6 DP showing anisotropic polarization luminescence phenomenon [32]. However, the crystal structure of bulk Cs_2KBiCl_6 is still an open question, as nanoscale materials often consist of surface defects in large amounts and take metastable structures differently from the bulk. This raises concerns about the structure and stability of Cs_2KBiCl_6. One might wonder whether Cs_2KBiX_6 DP is unstable like Cs_2AuBiX_6 given the similar ionic size and identical charge of K^+ and Au^+ (d^{10}) ions regardless of their different electronic configurations [33]. If Cs_2KBiX_6 DP is stabilized, it would be a good host material for Mn^{2+}-activated luminescence similar to $Cs_2NaBiCl_6$ DP [12]. Motivated by such an idea, we started an investigation on the Cs_2KBiCl_6 DPs. Here we report the isolation, crystal structure, and Mn^{2+}-activated luminescent of a new halide DP Cs_2KBiCl_6.

The initial synthesis attempt performed at ~503 K using the nominal composition of Cs_2KBiCl_6, led to a poor-crystalline DP with broad reflections in addition to secondary phases Cs_3BiCl_6 and KCl (Fig. S2 in Supporting information). Increasing the temperature above 573 K significantly improved the crystallinity of DP phase and reduced the secondary phases. Although the Cs_3BiCl_6 phase completely disappear at 853 K, a minor (~3%) KCl phase was still observable (Fig. S3 in Supporting information) and further confirmed through the segregation of potassium on the scanning electron microscope (SEM) image (Fig. S4 in Supporting information). By reducing 10% KCl in raw materials (Fig. S5 in Supporting information), the pure-phase DP sample was finally isolated at the nominal composition of $Cs_2K_{0.9}BiCl_{5.9}$ (or $Cs_{2.03}K_{0.92}Bi_{1.02}Cl_6$ equally).

SEM images and elementary analysis were recorded on the pellet $Cs_2K_{0.9}BiCl_{5.9}$ samples (Fig. S6 in Supporting information), showing homogeneous elements distributions. The Cs:K:Bi:Cl ratio of 2.37(7):0.94(6):1.05(6):5.64(1) in the sample essentially matches with the value in the stoichiometric DP phase Cs_2KBiCl_6. The excessive CsCl and $BiCl_3$ in the initial composition were either lost or formed amorphous during the reaction.

The XRD data of Cs_2KBiCl_6 sample can be well fitted with the $Cs_2NaBiCl_6$ structure model in Pawley mode (R_{wp} ~ 4.48%, Fig. S7a in Supporting information), indicating that Cs_2KBiCl_6 likely adopts an ideal DP structure as its Na analogue. However, the Rietveld refinement using the ideal DP structure model led to either extremely large B_{eq} (12.0–19.0 Å^2) for all atoms or large residue intensities (R_{wp} = 15.23%, Fig. S7b in Supporting information) with the constrained atomic $B_{eq} \leq 3.0$ Å^2. This indicates that these atoms deviate from the high-symmetric positions of ideal DP. Therefore, we amended the DP structural model slightly and allowed atomic shifts from ideal high-symmetric sites as well as fractional occupancy in the Rietveld refinement. This led to satisfactory fitting results with R_{wp} = 6.83% (Fig. 1a).

Due to their weak X-ray scattering ability, the light K^+ and Cl^- ions are not well located with X-ray diffractions in the presence of heavy elements such as bismuth and cesium. Neutron diffraction (ND) is more sensitive to identifying K^+ and Cl^- ions because the neutron scattering lengths of potassium (3.67 fm) and chloride (9.58 fm) are distinct from those of Cs (5.42 fm) and Bi (8.53 fm) [34]. Therefore, to find the accurate position of K^+ and Cl^-, neutron diffraction data were collected on the Cs_2KBiCl_6 sample. The weak diffused peaks on the ND data (Fig. 1b), *i.e.*, 3.0, 1.5 and 0.8 Å, indicate the likely presence of local ordering or amorphous phase in the Cs_2KBiCl_6 sample.

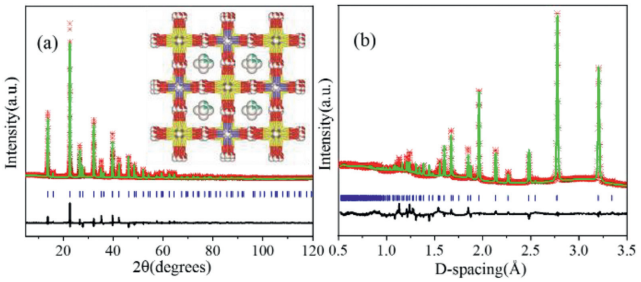

Fig. 1. Rietveld plots of (a) XRD data and (b) neutron data for Cs_2KBiCl_6. The inset to (a) shows a disordered DP structural model with the color code: blue sphere (Cs), red sphere (Cl), yellow sphere (K) and purple sphere (Bi).

Table 1
Final refined structural parameters for Cs_2KBiCl_6.

Atom	Site	*x*, *y*, *z*	Occupancy	B_{eq} (Å^2)
K	24*e*	0, 0, 0.0708(5)	0.1667	0.6(4)
Bi	24*e*	0.4703(1), 0, 0	0.1667	0.97(3)
Cs	48*g*	0.25, 0.25, 0.3049(1)	0.1667	1.82(7)
Cl	96*j*	0, 0.2665(1), −0.0435(1)	0.25	1.94(5)

a = 11.0895(1) Å, V = 1363.75(4) Å^3, space group: $Fm\bar{3}m$, Z = 4.

The Rietveld refinements were carried out against the XRD and neutron data simultaneously, using the disordered DP structural model. During the refinements, the preferred orientation of the sample was described with the spherical harmonic functions. The lattice parameters, atomic coordinates and B_{eq} parameters were refined. The final refinement converged to R_{wp} = ~6.83% and ~5.19% for XRD and ND data, as shown in Figs. 1a and b, respectively, and the refined structural parameters are listed in Table 1.

In the crystal structure of Cs_2KBiCl_6, the K, Bi, Cs, and Cl elements are shifted from the ideal DP sites with fractional occupancies in compensations (Fig. 1a inset). Among all the ions, the K^+ cation has the largest relative shift of ~7%, while Bi^{3+} has the smallest shift of ~3%. This indicates K^+ is an important factor for structural disorder as discussed in the following sections. The disordering of all ions in Cs_2KBiCl_6 prevents further meaningful structural analysis.

Quadrupolar ^{133}Cs (nuclear spin, I = 7/2, Qm = −0.34 fm^2) is a highly sensitive nuclear magnetic resonance (NMR) nucleus with excellent resolution, as it behaves as a pseudo spin-½ nucleus, rendering it ideal to investigate the local coordination environment. The ^{133}Cs magic angle spinning (MAS) NMR spectra for the Cs_2KBiCl_6 sample (Fig. 2a) consist of four resolved NMR resonances centered at 56(2), 121(2), 180(4), and 253(4) ppm with a ratio of 10:49:35:6 (fitted peak area). This indicates four distinct local coordination environments of Cs in the Cs_2KBiCl_6 material. Although only one 12-coordinated Cs site is present in the average structure, the fractional occupancy of Cs, Bi, K and Cl sites in Cs_2KBiCl_6 are compatible with different local environments of Cs. Due to their similar ionic size, the substitution of K^+ and Cs^+ is evitable in Cs_2KBiCl_6 DP and could lead to local connections and coordination numbers (CN) such as 7, 8 and 9 for Cs^+ ions similar to that in CsK_2BiCl_6 and Cs_3BiCl_6 materials (Fig. S8 in Supporting information). Furthermore, the ^{133}Cs peaks of Cs_2KBiCl_6 DP have full width at half maximum (FWHM) of 25.7–48.2 ppm and are much broader

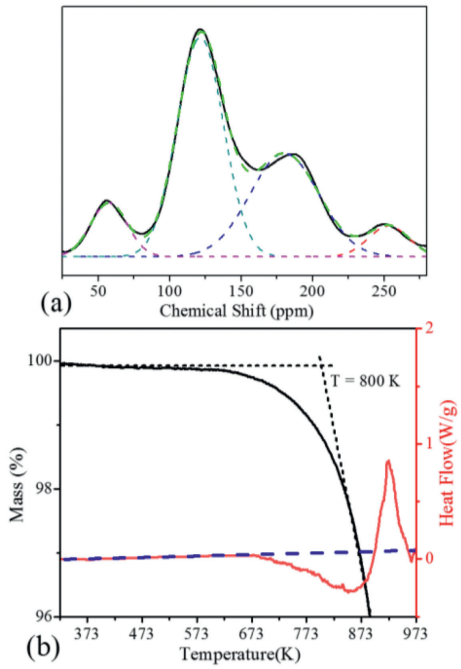

Fig. 2. (a) ^{133}Cs MAS NMR spectra (solid lines) and its overall best Gaussian fits (dotted lines) for Cs_2KBiCl_6. Spectra were acquired at a magnetic field strength of 9.4 T with a spinning frequency of 12 kHz. (b) TGA (black) and DTA (red) data for the Cs_2KBiCl_6 sample from room temperature (RT) to 973 K. The dashed baselines are shown in black and blue to guide the eyes for TGA and DTA, respectively.

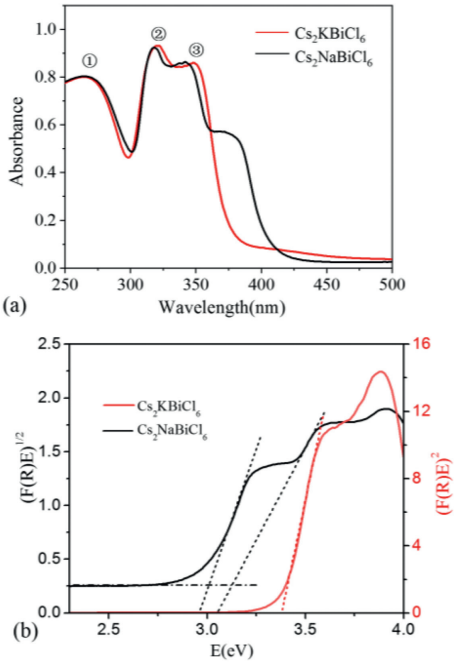

Fig. 3. (a) UV–vis absorption spectra and (b) the Tauc plot of Cs_2KBiCl_6 and $Cs_2NaBiCl_6$.

than those (FWHM = 1 ppm) of well-ordered DP $Cs_2AgInCl_6$ and $Cs_2AgBiCl_6$ [35]. This indicates the disorders of Cs ions in Cs_2KBiCl_6 are close to that in amorphous materials to some extent.

Thermal analysis and variable temperature X-ray diffraction (VT-XRD) experiments were carried out to examine the thermal stability of Cs_2KBiCl_6 in the air. During the thermal analysis, the Cs_2KBiCl_6 sample kept a constant weight below 573 K, as shown in the thermo gravimetric analysis (TGA) curve (Fig. 2b), which is consistent with VT-XRD data (Fig. S9 in Supporting information) showing that Cs_2KBiCl_6 was stable up to 523 K. In the TGA data, the initial weight loss starts at ~573 K and turns abrupt at ~800 K. These two temperatures are close to the melting point 506 K and boiling point 723 K of $BiCl_3$ [36], suggesting that the weight change was due to the loss of $BiCl_3$. The endothermic peak at 673–897 K is probably related to the decomposition, consistent with the arising of KCl reflections at 523–773 K in VT-XRD data. The decomposition was completed at 773 K, resulting in KCl and amorphous phases, as evidenced by the broad peaks in the 773 K XRD data. Upon further temperature increase from 773 K, this mixture transformed into other intermediate phases. This could explain the exothermic peak above 897 K, which was also associated with the significant loss of $BiCl_3$.

Low-temperature XRD patterns were collected to explore any possible phase change of Cs_2KBiCl_6 (Fig. S10a in Supporting information). No phase transition exists in the Cs_2KBiCl_6 material down to 5 K. Cs_2KBiCl_6 has a constant 3% volume decrease upon cooling from RT to 5 K. A smaller volume change (~2.5%) occurred when the sample was warmed from 5 K to RT at 1 K/min, although reversible volume increase was obtained at a warming rate of ~0.2 K/min (Fig. S10b in Supporting information). This history-dependent volume change indicates the slow relaxations in the Cs_2KBiCl_6 sample, also keeping with its disordered nature.

UV–vis diffuse reflectivity data (Fig. 3a) were collected and transformed into an optical absorbance coefficient $F(R)$ using the Kubelka-Munk equation; $F(R) = (1 - R)^2/2R$, where R is the reflectance [37]. Similar to that of $Cs_2NaBiCl_6$, the absorption curve of Cs_2KBiCl_6 consists of three distinct peaks at 270, 321 and 349 nm, all associated with a $6s^2$–$6s^1p^1$ transition of the localized $[BiCl_6]^{3-}$ octahedron. Precisely, the peak at a shorter wavelength ~270 nm (band 1) is assigned to the $^1S_0 \rightarrow {}^3P_2$ partially allowed transition; The double peaks centered at 321 and 349 nm (bands 2 and 3) are related to the $^1S_0 \rightarrow {}^3P_1$ spin-forbidden transition.

The absorption edge of Cs_2KBiCl_6 DP around 349 nm are sharp and intense, indicating a probable direct band-gap, which can be obtained on the Tauc plot as the intercept from the linear fits to the $[F(R)E]^2$. From the corresponding Tauc plot (Fig. 3b), the direct gaps of Cs_2KBiCl_6 can be estimated to be ~3.35 eV, agreeing with theoretical value (~3.18 eV) of Cs_2KBiCl_6 (Fig. S11 in Supporting information). While the fitting to $[F(R)E]^{1/2}$ leads to an indirect gap of 3.1 eV for $Cs_2NaBiCl_6$, matching well with the reported value (3.41 and 3.19 eV) [38–40]. An extrinsic defect-related subband gap is estimated to be ~3.02 eV for $Cs_2NaBiCl_6$ [25,38].

The conduction band minimum (CBM) is split off from other conduction bands due to the strong SOC interactions of the Bi 6p states. While the valence band maximum (VBM) is originated from the hybridization of the Bi 6s and Cl 3p states, as seen from the corresponding charge densities shown in Fig. S12 (Supporting information).

Cs_2KBiCl_6 samples were doped by Mn^{2+} according to two Mn replacing K and Bi (*i.e.*, $Cs_2K_{1-x}Bi_{1-x}Mn_{2x}Cl_6$). All the Mn-doped samples $Cs_2K_{1-x}Bi_{1-x}Mn_{2x}Cl_6$ ($x = 0$, 0.004, 0.007, 0.01, 0.02, 0.025, 0.05) exhibit similar XRD patterns (Fig. S13 in Supporting information). The Rietveld refinement against the XRD data of the highly Mn-doped composition $x = 0.025$ was performed with different structural models. The best fit was obtained with the model in which Mn equally substituted on both the K and Bi sites (Fig. S14 in Supporting information, $R_{wp} = 6.50\%$), compared with those where Mn substituted on the Bi or K site only ($R_{wp} = 6.64\%$ and 6.80% respectively). This indicates that Mn(II) ions prefer entering both K and Bi sites. Magnetization measurements were performed on the $x = 0.025$ sample, which was paramagnetic and consistent with the diluted manganese ions in the host lattice. The Curie-Weiss fitting was performed on the 2–12 K data with the most pro-

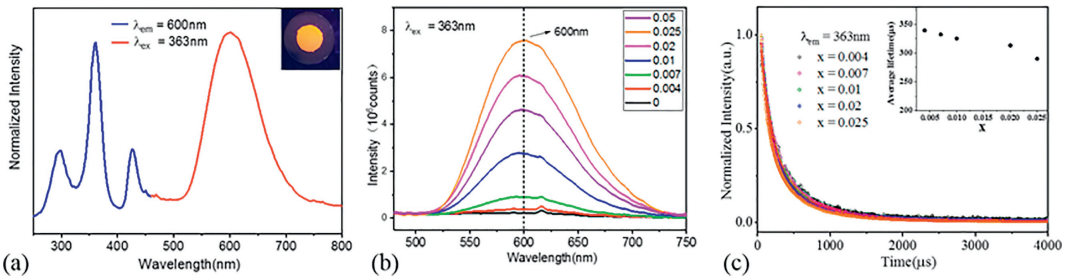

Fig. 4. (a) Excitation (blue) and emission (red) spectra for the $x = 2.5\%$ Mn-doped Cs_2KBiCl_6 sample, with its photograph taken under 365 nm illumination shown in the inset. (b) Emission spectra of $Cs_2K_{1-x}Bi_{1-x}Mn_{2x}Cl_6$ ($x = 0$–0.05) samples under an excitation wavelength of 363 nm. (c) Luminescent decay curves of the $^4T_1 \rightarrow {}^6A_1$ transition of Mn^{2+} in the $Cs_2K_{1-x}Bi_{1-x}Mn_{2x}Cl_6$ samples. The symbols correspond to the experimental data, while the lines show the fitted double-exponential dependence. The inset shows the average lifetime for all the Mn-doped Cs_2KBiCl_6 samples.

nounced paramagnetic signal (Fig. S15 in Supporting information). The fits resulted in an effective moment of 5.7(1) μ_B per Mn, essentially identical to that of 5.9 μ_B for a high spin (HS) Mn^{2+} ion, thus confirming that the incorporated Mn is Mn^{2+} in HS state.

The Mn^{2+}-doped Cs_2KBiCl_6 sample shows orange-red photoluminescence with a medium-wide emission band centered at 600 nm (Fig. 4a). The emission originates from a $^4T_1 \rightarrow {}^6A_1$ transition of octahedrally coordinated Mn^{2+} centers and shows CIE coordinates of $x = 0.53$ and $y = 0.42$, which are slightly red-shifted from those of the Na counterpart ($x = 0.51$ and $y = 0.44$). The change in chromaticity can be observed in the CIE diagram plotted in Fig. S16 (Supporting information). When no dopant is added, the Cs_2KBiCl_6 material exhibits very weak luminescence centered at ~615 nm from the Bi^{3+} ions located near the defect site. The emission intensity of $Cs_2K_{1-x}Bi_{1-x}Cl_6$ increases with the increasing Mn content within the range of $x = 0$–0.025 (Fig. 4b).

The excitation spectrum for the $x = 0.025$ member (Fig. 4a) shows peaks centered at 297, 363, and 425 nm, slightly red-shifted compared with its Na analogue. These bands do not match the absorption bands observed in the UV–vis spectra of the parent material (Fig. S17 in Supporting information), so we assign them to the direct excitation of the electrons from the Mn^{2+} ground state $^6A_1(6S)$ to higher levels of the 3d manifold, *i.e.*, $^4T_1(4P)$, $^4T_2(4D)$, and $^4T_2(4G)$. Thus, the absence of absorption bands due to the spin-forbidden $^1S_0 \rightarrow {}^3P_{1,2}$ transitions of Bi^{3+} in the excitation spectrum, where the emission of Mn^{2+} is being monitored, proves that the resulting emission is not sensitized by the host.

To find out the optimal dopant concentration, the decay of the emission originated from the $^4T_1 \rightarrow {}^6A_1$ transition (at ~600 nm) was recorded for all the Mn^{2+}–doped samples (Fig. 4c). The PL decay curves have been described by the following biexponential function:

$$I(t) = I_1 \exp\left(-\frac{t}{\tau_1}\right) + I_2 \exp\left(-\frac{t}{\tau_2}\right) \quad (1)$$

where $I(t)$ is the luminescence intensity, t is the time after excitation, and τ_i ($i = 1, 2$) is the decay time of the i^{th} component, with intensity I_i. This is reasonable since Mn simultaneously replaces both K and Bi sites, which are crystallographically inequivalent and may lead to two different luminescence relaxations, similar to that in the $Cs_2LiBiCl_6$: Mn materials. The average decay times $\langle\tau\rangle$, calculated according to the following equation (Eq. 2) have been plotted in Fig. 4c inset.

$$\langle\tau\rangle = \frac{\int_0^\infty tI(t)\,dt}{\int_0^\infty I(t)\,dt} = \frac{\tau_1^2 I_1 + \tau_2^2 I_2}{\tau_1 I_1 + \tau_2 I_2} \quad (2)$$

As observed, $\langle\tau\rangle$ slightly decreases monotonously from 339 μs to 290 μs when the Mn^{2+} content increases from 0.4% to 2.5%, although a clear quenching effect cannot be observed within the compositional range analyzed. Similar magnitude of lifetime has been reported in halide perovskite [41]. Photoluminescence quantum yield (PLQY) measurements were then performed at an excitation wavelength of 363 nm and indicated a maximum of ~15.8% in the $x = 0.02$ sample (Table S1 in Supporting information), similar to that in $Cs_2NaBiCl_6$:Mn materials. The $x = 0.004$ sample has the minimum PLQY of ~4.7%, close to that of $Cs_2AgInCl_6$:Mn materials. Although the more efficient phosphor has been found for the $x = 0.02$ composition, from a practical view, the most interesting composition is the one doped with 2.5 mol% Mn^{2+} as it exhibits the highest emission intensity (Fig. 4b) owing to the larger number of emission centers compensate for the concentration quenching effect.

Temperature-dependent emission spectra (Fig. S18a in Supporting information) were collected for the $x = 0.025$ sample upon 363 nm excitation to evaluate the luminescence thermal quenching behavior of the material. The decrease in the emission intensity as well as a blue shift of the emission is observed with increasing temperature, which is normally ascribed to the enhanced nonradiative transition probability and crystal lattice strain. When the temperature rose to 200 and 300 K, the emission intensity of the orange emission can maintain ~65% and ~9% of its initial value (at 95 K), showing obvious thermal quenching behavior (Fig. S18b in Supporting information). The emission almost disappears at 360 K, indicating that the Cs_2KBiCl_6: Mn materials may not be suitable for application in pc-LED which typically achieve 400–450 K near the LED chip [42].

Two empirical criteria, the Goldschmidt tolerance factor (*TF*) [43] and the octahedral factor (μ) are popular to assess the stability of the perovskite halides. They are defined as $TF = (R_A + R_X)/\sqrt{2}(R_M + R_X)$ and $\mu = R_M/R_X$, where R_A, R_M, and R_X represent the ionic radii of A, M and X ions. Statistical analysis on simple perovskites indicates that stable halide perovskites have TF and μ in the range of 0.87–1.1 and 0.414–0.732 respectively [44]. This empirical relationship can be extended to the $Cs_2M^IM^{III}Cl_6$ DPs when the average ionic radii of M^I and M^{III} are adopted as R_M. Employing the Shannon ionic radii of 12-coordinated Cs^+ (1.88 Å) and 6-coordinated M^I, M^{III}, and Cl^- (1.81 Å) ions [45], the calculated *TF* and μ values of all the experimentally stabilized DPs $Cs_2M^IM^{III}Cl_6$ ($M^I = Li^+$, [25,30,46,47] Na^+, [11,47–51] Ag^+ [4,23,52-54], Au^+ [54,55], Tl^+ [56] and K^+ [30,31], $M^{III} = In^{3+}$, Tl^{3+}, Sb^{3+}, Au^{3+}, Bi^{3+} and *RE*) falls in the empirical stable area, as listed in Table 2. However, for larger M^I cations such as K^+, Tl^+ and Au^+, which prefer to take more than six Cl^- ions, the octahedral factor of the M^ICl_6 octahedron (0.76–0.83) is out of the empirical criterion, and the *TF* of $Cs_2M^IM^{III}Cl_6$ (0.87–0.90) is on the lower limit of the empirical criterion. Therefore, $Cs_2M^IM^{III}Cl_6$ ($M^I = K^+$, Tl^+ and Au^+) often adopt distorted DP structures in low symmetry rather than ideal DP structures as other $Cs_2M^IM^{III}Cl_6$ ($M^I = Li^+$, Na^+ and Ag^+) DPs. Indeed, the low-symmetric structural distortion helps to meet the higher-coordination requirement of large M^I

Table 2
Experimentally stabilized $Cs_2M^IM^{III}Cl_6$ DPs showing tolerance factor *TF* and octahedral factor μ.

Compound	(μ, *TF*)	Compound	(μ, *TF*)
$Cs_2LiBiCl_6$ [25]	(0.49, 0.97)	$Cs_2AgBiCl_6$ [4]	(0.60, 0.90)
Cs_2LiYCl_6 [46,47]	(0.46, 0.99)	$Cs_2AgInCl_6$ [23,52]	(0.54, 0.94)
$Cs_2LiLuCl_6$ [30]	(0.45, 1.00)	$Cs_2AgTlCl_6$ [53]	(0.56, 0.92)
$Cs_2NaInCl_6$ [48,49]	(0.50, 0.96)	$Cs_2AgSbCl_6$ [23]	(0.53, 0.94)
$Cs_2NaBiCl_6$ [11]	(0.57, 0.92)	$Cs_2AgAuCl_6$ [54]	(0.55, 0.93)
$Cs_2NaSbCl_6$ [49]	(0.49, 0.97)	Cs_2KBiCl_6	(0.67, 0.87)
$Cs_2NaRECl_6$ (*RE* = Y, Sc, La−Gd, Dy, Er, Tm, Lu, Bk, U) [47,49-51]	(0.45∼0.52, 0.91∼0.96)	Cs_2KRECl_6 (*RE* = Sc, Eu, Tb) [30,31]	(0.54∼0.64, 0.88∼0.90)
$Cs_2TlTlCl_6$ [56]	(0.66, 0.87)	$Cs_2AuAuCl_6$ [54,55]	(0.61, 0.89)

cations. Meanwhile, due to the similar radius, Cs^+ and K^+ (1.64 Å, CN = 12) could substitute each other inevitably in the Cs_2KBiCl_6 DP. However, the substitution could destabilize the double perovskite phase and form a local non-perovskite connection, as indicated by the fact that 50% of Cs replaced by K leads to cryolite CsK_2BiCl_6, while the replacement of K by Cs results in cryolite Cs_3BiCl_6. Furthermore, due to the $6s^2$ lone pair, the Bi^{3+} ion prefers local asymmetric coordination rather than octahedron in DP halides, which further enhances the structural distortion. This often leads to large atomic thermal displacements (B_{eq} = 0.9–3.1 Å^2) in the cubic structure of Bi-based halides $Cs_2M^IBiCl_6$ ($M^I = Li^+$, Na^+ and Ag^+) [4,11,25]. Overall, both factors large-sized K^+ and Bi^{3+} with $6s^2$ lone pair contribute to the enhanced structural distortion of Cs_2KBiCl_6 DP, forming a disordered cubic crystal structure with complex local coordination environments.

In summary, a new bismuth-based DP halide Cs_2KBiCl_6 was synthesized successfully. From combined Rietveld refinement against the XRD and NPD data, its crystal structure consists of shifted Cs, K, Bi, and Cl sites from the ideal positions with fractional occupancy in compensation. Four distinct local coordination of Cs^+ ions are revealed in Cs_2KBiCl_6 by ^{133}Cs solid-state nuclear magnetic resonance spectroscopy. The Cs_2KBiCl_6 DP displays thermal-history-dependent volume change at the 5–298 K range. The Cs_2KBiCl_6 has a direct band gap of 3.35(2) eV and red-shift luminescence around 600 nm upon Mn doping compared with the Na analogue. The disordered structure of Cs_2KBiCl_6 is stabilized via two factors, large K^+ cations which prefer to bond with more than six Cl^-, and the Bi^{3+} with $6s^2$ lone pair which has a preference for a local asymmetric environment.

Declaration of competing interest

The authors declare that they have no known competing financial interests or personal relationships that could have appeared to influence the work reported in this paper.

Acknowledgments

The authors thank the National Science Foundation of China (Nos. 22090043 and 22161014), Guangxi Natural Science Foundation (Nos. 2019GXNSFGA245006 and 2020GXNSFAA297220), and the Foundation of Guilin University of Technology (No. GUTQDJJ2018115) for the financial support.

Supplementary materials

CSD 2,160,488 contains the supplementary crystallographic data for this paper. The data can be obtained free of charge via www.ccdc.cam.ac.uk/data_request/cif, or by emailing datarequest@ccdc.cam.ac.uk, or by contacting The Cambridge Crystallographic Data centre, 12 Union Road, Cambridge CB2 1EZ, U.K.; fax: + 44 1223 336,033.

Supplementary material associated with this article can be found, in the online version, at doi:10.1016/j.cclet.2023.108641.

References

[1] A. Kojima, K. Teshima, Y. Shirai, et al., J. Am. Chem. Soc. 131 (2009) 6050–6051.
[2] X. Sun, D. Zhao, Z.a. Li, Chin. Chem. Lett. 29 (2018) 219–231.
[3] A.K. Jena, A. Kulkarni, T. Chem. Rev. 119 (2019) 3036–3103.
[4] E.T. McClure, M.R. Ball, et al., Chem. Mater. 28 (2016) 1348–1354.
[5] C.N. Savory, A. Walsh, D.O. Scanlon, ACS Energy Lett. 1 (2016) 949–955.
[6] A.H. Slavney, T. Hu, A.M. Lindenberg, et al., J. Am. Chem. Soc. 138 (2016) 2138–2141.
[7] R.L. Hoye, L. Eyre, F. Wei, et al., Adv. Mater. Interfaces 5 (2018) 1800464.
[8] W. Pan, H. Wu, J. Luo, et al., Nat. Photonics 11 (2017) 726–732.
[9] S. Wang, Y. Xie, W. Jiang, et al., Chin. Chem. Lett. 34 (2023) 108521.
[10] F. Wei, Z. Deng, S. Sun, et al., Chem. Commun. 55 (2019) 3721–3724.
[11] L.R. Morss, W.R. Robinson, Acta Cryst. B 28 (1972) 653–654.
[12] J.D. Majher, M.B. Gray, T.A. Strom, et al., Chem. Mater. 31 (2019) 1738–1744.
[13] H. Yang, Y. Guo, G. Liu, et al., Chin. Chem. Lett. 33 (2022) 537–540.
[14] J. Luo, S. Li, H. Wu, et al., ACS Photonics 5 (2018) 398–405.
[15] J. Glodo, R. Hawrami, K.S. Shah, J. Cryst. Growth 379 (2013) 73–78.
[16] H. Shi, M.H. Du, Phys. Rev. Appl. 3 (2015) 054005.
[17] J. Luo, X. Wang, S. Li, et al., Nature 563 (2018) 541–545.
[18] A. Zhang, Y. Liu, G. Liu, et al., Chem. Mater. 34 (2022) 3006–3012.
[19] Y. Liu, X. Rong, M. Li, et al., Angew. Chem. Int. Ed. 59 (2020) 11634–11640.
[20] Y. Liu, M.S. Molokeev, Z. Xia, Energy Mater. Adv. 2021 (2021) 2585274.
[21] Q. Jia, T. Shao, L. Tong, et al., Chin. Chem. Lett. 34 (2023) 107539.
[22] A.H. Slavney, L. Leppert, D. Bartesaghi, et al., J. Am. Chem. Soc. 139 (2017) 5015–5018.
[23] T.T. Tran, J.R. Panella, J.R. Chamorro, et al., Mater. Horiz. 4 (2017) 688–693.
[24] K.P. Lindquist, S.A. Mack, A.H. Slavney, et al., Chem. Sci. 10 (2019) 10620–10628.
[25] Y. Sun, A.J. Fernández-Carrión, Y. Liu, et al., Chem. Mater. 33 (2021) 5905–5916.
[26] P. Vishnoi, R. Seshadri, A.K. Cheetham, J. Phys. Chem. C. 125 (2021) 11756–11764.
[27] S.E. Creutz, E.N. Crites, M.C. De Siena, Nano Lett. 18 (2018) 1118–1123.
[28] C. Zhang, L.G. Gao, S. Teo, et al., Sustain. Energy Fuels 2 (2018) 2419–2428.
[29] Z.W. Xiao, K.Z. Du, W.W. Meng, et al., Angew. Chem. Int. Ed. 56 (2017) 12107–12111.
[30] G. Meyer, S.J. Hwu, J.D. Corbett, Z. Anorg. Allg. Chem. 535 (1986) 208–212.
[31] M. Villafuerte-Castrejón, M. Estrada, J. Gomez-Lara, et al., J. Solid State Chem. 132 (1997) 1–5.
[32] C. Wang, M. Sun, H. Wang, et al., J. Phys. Chem. Lett. 14 (2023) 164–169.
[33] C.J. Bartel, J.M. Clary, C. Sutton, et al., J. Am. Chem. Soc. 142 (2020) 5135–5145.
[34] V.F. Sears, Neutron News 3 (1992) 26–37.
[35] A. Karmakar, G.M. Bernard, A. Meldrum, et al., J. Am. Chem. Soc. 142 (2020) 10780–10793.
[36] P. Patnaik, Handbook of Inorganic Chemicals, McGraw-Hill Companies, Inc., New York, 2002, pp. 1–1125.
[37] D.B. Judd, J. Res. Nat. Bur. Standards 13 (1934) 281–291.
[38] S. Wu, W. Li, J. Hu, et al., J. Mater. Chem. C. 8 (2020) 13603–13611.
[39] J. Zhou, X.M. Rong, P. Zhang, et al., Adv. Opt. Mater. 7 (2019) 1801435.
[40] X.G. Zhao, J.H. Yang, Y.H. Fu, et al., J. Am. Chem. Soc. 139 (2017) 2630–2638.
[41] C. Wang, L. Ma, S. Wang, et al., J. Phys. Chem. Lett. 12 (2021) 12129–12134.
[42] P.F. Smet, A.B. Parmentier, D. Poelman, J. Electrochem. Soc. 158 (2011) R37–R54.
[43] V.M. Goldschmidt, Naturwissenschaften 14 (1926) 477–485.
[44] C. Li, X. Lu, W. Ding, et al., Acta Cryst. B 64 (2008) 702–707.
[45] R.D. Shannon, Acta Cryst. A 32 (1976) 751–767.
[46] C. Combes, P. Dorenbos, C. Van Eijk, et al., J. Lumin. 82 (1999) 299–305.
[47] C. Reber, H.U. Guedel, G. Meyer, et al., Inorg. Chem. 28 (1989) 3249–3258.
[48] P. Han, X. Mao, S. Yang, et al., Angew. Chem. Int. Ed. 58 (2019) 17231–17235.
[49] L.R. Morss, M. Siegal, L. Stenger, et al., Inorg. Chem. 9 (1970) 1771–1775.
[50] M. Spirlet, J. Rebizant, J. Fuger, Acta Cryst. C 44 (1988) 1300–1301.
[51] L.R. Morss, J. Fuger, Inorg. Chem. 8 (1969) 1433–1439.
[52] G. Volonakis, A.A. Haghighirad, R.L. Milot, et al., J. Phys. Chem. Lett. 8 (2017) 772–778.
[53] A.H. Slavney, L. Leppert, A.S. Valdes, et al., Angew. Chem. Int. Ed. 57 (2018) 12765–12770.
[54] N. Elliott, L. Pauling, J. Am. Chem. Soc. 60 (1938) 1846–1851.
[55] X.J. Liu, K. Matsuda, Y. Moritomo, et al., Phys. Rev. B 59 (1999) 7925–7930.
[56] M. Retuerto, T. Emge, J. Hadermann, et al., Chem. Mater. 25 (2013) 4071–4079.